Fliri, Lukas; Guizani, Chamseddine; Miranda-Valdez, Isaac Yair; Pitkänen, Leena; Hummel, Michael

Reinvestigating the concurring reactions in early-stage cellulose pyrolysis by solution state NMR spectroscopy

Published in:
Journal of Analytical and Applied Pyrolysis

DOI:
10.1016/j.jaap.2023.106153

Published: 01/10/2023

Document Version
Publisher's PDF, also known as Version of record

Please cite the original version:
Fliri, L., Guizani, C., Miranda-Valdez, I. Y., Pitkänen, L., & Hummel, M. (2023). Reinvestigating the concurring reactions in early-stage cellulose pyrolysis by solution state NMR spectroscopy. *Journal of Analytical and Applied Pyrolysis*, *175*, Article 106153. https://doi.org/10.1016/j.jaap.2023.106153

Journal of Analytical and Applied Pyrolysis 175 (2023) 106153

Contents lists available at ScienceDirect

Journal of Analytical and Applied Pyrolysis

journal homepage: www.elsevier.com/locate/jaap

Reinvestigating the concurring reactions in early-stage cellulose pyrolysis by solution state NMR spectroscopy

Lukas Fliri [a], Chamseddine Guizani [b,*], Isaac Yair Miranda-Valdez [a], Leena Pitkänen [a], Michael Hummel [a,*]

[a] *Department of Bioproducts and Biosystems, Aalto University, P.O. Box 16300, 0076 Aalto, Finland*
[b] *VTT Technical Research Centre of Finland, Tietotie 2, FI-02150 Espoo, Finland*

ARTICLE INFO

Keywords:
Cellulose carbonization
Low temperature
Pre-treatment
Char yield
Active cellulose

ABSTRACT

Low temperature pre-treatments increase the char yield during cellulose carbonization. Although this effect is mostly understood on a kinetic basis, the formed chemical structures leave room for scrutiny. In ongoing ambitions to enhance the char yield of bioderived precursors, the thereby occurring chemistry was reinvestigated. A set of isothermal heating protocols ranging from 150° to 250°C was applied to man-made Ioncell® cellulose fibers and to Avicel® PH-101 microcrystalline cellulose. The prepared cellulosic samples were examined by solution state NMR using a tetra-*n*-butyl phosphonium acetate ($[P_{4444}][OAc]$): DMSO-d_6 (1:4 wt%) electrolyte as dissolving medium. Complementary, IR spectroscopy, size-exclusion chromatography (SEC) and thermogravimetric analysis coupled with mass spectroscopy (TGA-MS) measurements were performed. The NMR spectra evidenced the formation of levoglucosan end capped moieties as being the first and major occurring reaction during low temperature pre-treatments. In contrast to other mechanistic proposals, no signs for carbonyl or alkene functionalities were discernible in the cellulosic material soluble in the NMR electrolyte, even after treatment at 250 °C for several hours. Thermal cross-linking was observed in SEC already at temperatures not known to significantly influence the overall char yield. In the solution state analytics only partial solubility was observed, owing to the formation of a reluctant fraction previously described as “thermostable condensed phase”. This resulted in analytical blind spots and led to discrepancies between NMR results and FTIR spectra in which carbonyl and alkene vibrations were clearly discernible. Those discrepancies might also imply the co-existence of different fractions in the early stages of cellulose pyrolysis.

1. Introduction

Pyrolysis of biomass has received a considerable amount of research interest in the last decades in ambitions to convert renewable feedstocks to bioderived chemicals and materials [1–12]. Cellulose as the most abundant biopolymer has been studied extensively and often served as a model compound to understand the complex molecular and supramolecular transformations during high temperature treatment of lignocellulosic substrates. It was found that cellulose undergoes two competing pathways leading either to the formation of valuable, volatile low molecular weight compounds, with levoglucosan as its major constituent, or to char as solid residue in combination with the release of H_2O, CO and CO_2. When only applying inert conditions and no chemical pre-treatments, the heating rate was identified as an important factor to control the outcome of the reaction, with high heating rates favoring the production of volatile low molar mass fractions, and low heating rates increasing the char yield [13,14].

The two-pathway model, also termed as Broido-Shafizadeh model, was established following thorough investigations made in the 1960 s and ‘70 s [13–19]. The temperature range from 150° to 250°C was identified as the most significant for the final product distribution. Although both Broido and Shafizadeh left room for scrutiny in the discussion of their results and the model was challenged several times [20,21], it was found to adequately describe the occurring processes on a kinetic basis, and it is – with some adjustments – still widely accepted until today [22]. In this model, the observed product distribution was connected to the formation of so called “active cellulose” as a key intermediate in the low temperature pretreatments. Despite exhaustive research, the exact composition or mere existence of “active cellulose” is still controversially discussed in the pyrolysis community [23]. The

---

* Corresponding authors.
E-mail addresses: chamseddine.guizani@vtt.fi (C. Guizani), michael.hummel@aalto.fi (M. Hummel).

https://doi.org/10.1016/j.jaap.2023.106153
Received 11 July 2023; Received in revised form 22 August 2023; Accepted 28 August 2023

conducted investigations heavily relied on thermal analysis [20,24–34]. For the more thoroughly investigated volatile lower molar mass fractions formed in the non-char forming pathway they were eventually connected with chromatography or mass spectroscopy tools [35–37]. Inherently, these techniques only gave limited information on the solid residue. Investigations on the solid fractions relied on material characterization or chemical solid state spectroscopic techniques, like Fourier transform infrared (FTIR) or solid state ^{13}C NMR spectroscopy [23]. Thereby, the offered resolution to unambiguously clarify the occurring chemical transformations in the relevant temperature range was too low. There were obvious changes in the FTIR spectra, but they were still dominated and heavily superimposed by the cellulose vibrations [38]. In solid state ^{13}C NMR spectra of heat-treated cellulose changes in the supramolecular interactions were detected [39], but there were almost no discernable chemical changes up to a temperature of 250 °C [35]. Further insights could only be obtained in samples treated at higher temperatures [35,40–42]. However, treatments at these harsher conditions were reported to be less significant for the overall char yield [43].

Considering that water represents one of the first detectable generated analytes in the respective temperature range of 150 – 250 °C, the transformations were often connected to dehydration reactions directly from the anhydroglucose units (AGU) in the cellulose backbone [44]. It is reasonable to believe that one of these structures is responsible for the discrimination between the two competing pathways leading to lower or higher char yields. A reaction scheme postulating the major transformations in the low temperature region was summarized by Tang and Bacon in 1964 based on an IR study (Scheme 1A) [38]. It was proposed, that after removal of physically adsorbed H_2O and a concomitant chain scission leading to a reduction of the degree of polymerization (DP) until a level-off DP is reached, a further dehydration step leads to release of H_2O from the AGU. The proposedly formed keto-anhydroglucose structure can thereafter diverge into the two pathways. Either a levoglucosan (LGA) end capped moiety is formed following another chain scission and mainly leading to the generation of volatile lower molecular weight fractions, or a double bond is generated following a further removal of H_2O from the AGU and predominantly resulting in the

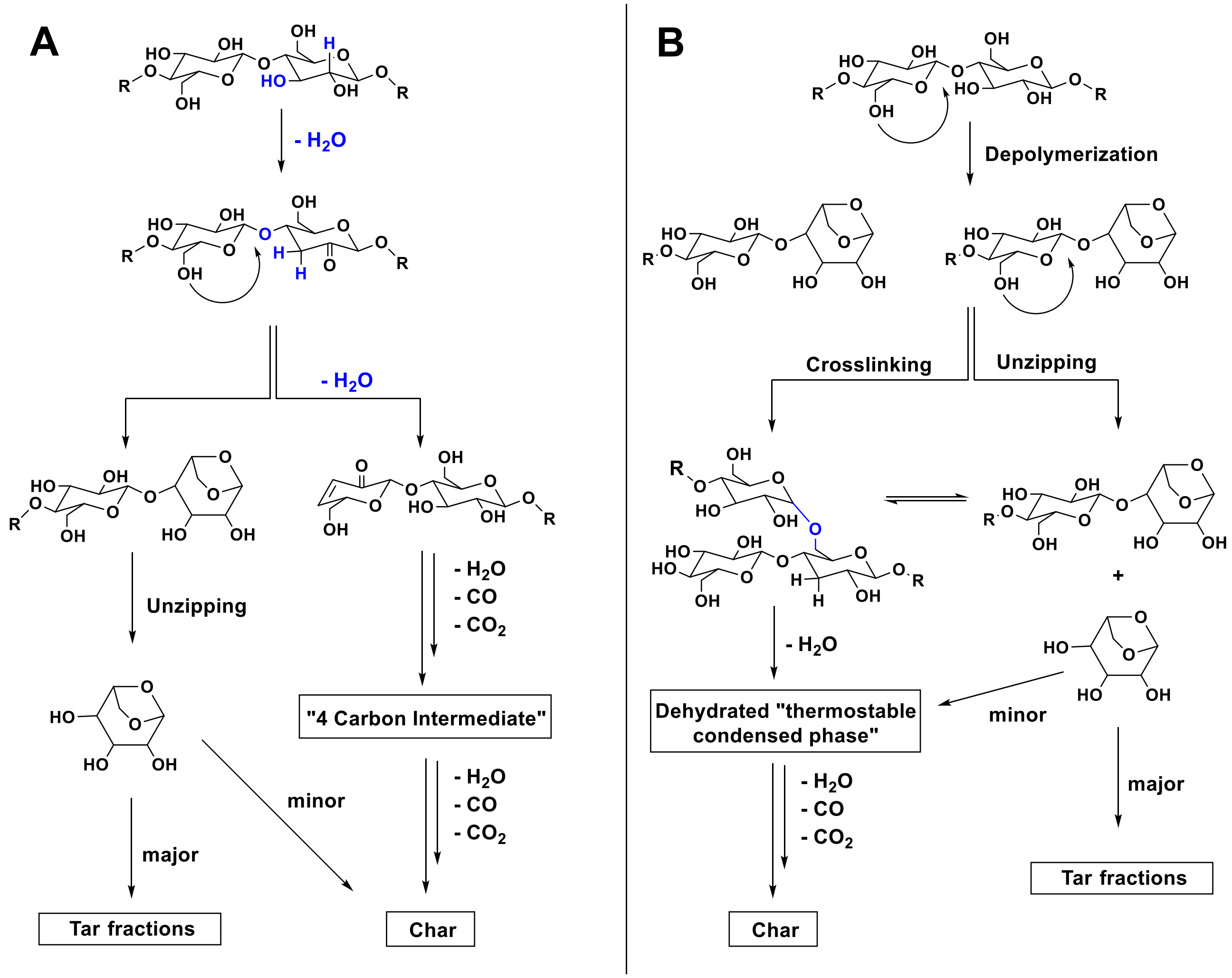

Scheme 1. Different reactions postulated in heat pretreatments of cellulose in the temperature range of 150 – 250 °C, which were reinvestigated in this study. **A)** Following IR investigations, Tang and Bacon proposed the formation of dehydrated carbonyl bearing AGU structures as key intermediates in the discrimination between the two known pyrolysis pathways [38]. Either further dehydration to alkene bearing moieties mainly leads to char formation, or formation of levoglucosan end-capped structures predominantly leads to tar formation following further "unzipping" of the polymer chain. **B)** Attempt to summarize different literature reports which highlighted the importance of the thermal polymerization in char formation - presumably *via* levoglucosan end capped structures - to a reaction scheme. LGA end capped cellulosics are postulated as predominantly formed intermediate in the low temperature treatment. Discrimination between the two pathways can be explained through concurring depolymerization and repolymerization reactions. Complete depolymerization yields LGA containing tar as major product. The repolymerization results in the introduction of different glycosidic bonds, weakening of the rigid H-bonds in the crystallites and results in a less thermally stable polysaccharide. This can undergo dehydration reactions to a not well understood "thermostable condensed phase" [35] ultimately resulting in the formation of char. **R** = H or cellulose chain.

formation of a carbonaceous solid residue. Although, this model is in line with the kinetic observations the postulated chemical reactions or the proposed dehydrated cellulose structures could so far not be cross validated using other analytical techniques than IR spectroscopy. Nonetheless, this reaction scheme is still widely accepted and cited especially in studies focusing on the generation of carbons from cellulose [44,45]. Presumably, this is due to the common application of water withdrawing compounds like sulphates or phosphates to increase the char yield during carbonization, which would be in accordance with this dehydration mechanism [46–48].

Nonetheless, the scheme is far from being generally accepted. For example, Michael J. Antal, who significantly contributed to advancing the understanding of cellulose pyrolysis, highlighted other phenomena in a still outstanding normative review summarizing the knowledge about carbohydrate pyrolysis up to the early 1980 s [49]. He concluded that condensation or polymerization reactions dominate the pyrolysis phenomena below 250 °C and ultimately result in the formation of char, CO_2, CO and H_2O [49]. Thermal crosslinking reactions in cellulose heat treatment were noted early on and were connected to the occurrence of a “thermostable condensed phase” [35,50]. Thereby both a radical [51, 52] and a cationic progression [49] [53] of the reaction was proposed. Again, an exact mechanistic background of the polymerization / condensation was not accepted. More recently the importance of LGA-end capped structures and LGA in general in char formation was pointed out [54–58], although the same structures were more commonly connected to the formation of volatiles over unzipping reactions [38]. Theoretical computations also suggested the formation of LGA-end capped cellulose structures as energetically most favorable thermal transformation [59]. The thermal polymerization of LGA was often investigated, *e.g.*, in the context of pyrodextrin formation [60–62] and the similarities between the chars obtained from LGA and cellulose carbonization were pointed out [63]. The occurrence of more reactive anhydroglucose structures obtained from internal isomerization was also evidenced after low temperature treatment of other (poly)saccharides which were easier to analyze [49] and were also connected to char formation [64]. The increased char yield after isothermal treatment of cellulose at low temperatures can thus be explained through partial depolymerization through unzipping leading to the formation of LGA end capped structures, which subsequently repolymerize and dehydrate to a complex scaffold ultimately leading to char formation. However, to the best of our knowledge there was so far no attempt to postulate an alternative reaction mechanism based on these observations. Furthermore, the reactions ultimately leading to dehydration or the thereby formed structures are not addressed therein. An attempt to outline some of the concurring reactions is summarized in Scheme 1B.

In conclusion, despite the longstanding research interest, the occurring reactions are still controversially discussed. This can be partly seen as a consequence of the limited resolution of the analytics available to examine the chemical transformations in the treated fractions. In our research group efforts to use man made cellulosic Ioncell® fibers as starting material to produce carbon fibers [65–68], the inherently low char yields represent an everlasting problem. Isothermal low temperature pretreatments over several hours were reported to drastically increase the obtainable char yield [43]. Thereby, the range of 230 – 250 °C was identified as the most important temperature area, while milder (215 °C) or harsher (270 °C) isothermal treatments did not significantly influence the outcome [43]. In this sense, we were interested in a better understanding of the mechanistic background and of the formed structures, as these could open new entry points for chemical pretreatment strategies in cellulose carbon fiber production. For this endeavor, the applicability of a recently proposed solution state NMR protocol for cellulosic materials using a tetra-*n*-butylphosphonium acetate ([P_{4444}][OAc]) – DMSO-d_6 (1:4 wt%) electrolyte was tested in this study [69–71]. Compared to the often-reported solid state NMR analytics [35, 40–42], this technique offered significantly higher resolution and the possibility to perform more peculiar 2D NMR experiments, including multiple bond correlated ones. Another in-solution protocol was used to monitor the development of the molecular weight distributions (MWDs) through size exclusion chromatography (SEC). While these techniques offer in-depth information, solubility of the cellulosic material is a prerequisite to allow for the analysis. This proved to be problematic owing to the supramolecular and chemical changes introduced by the harsh treatments. While it was possible to analyze all samples, other analytical techniques like FTIR and STA-MS were used for cross validation and to address the blind spots of the solution state procedures.

2. Materials and methods

2.1. Starting material

The study was conducted with standard Ioncell® fibers spun from dissolving grade pre-hydrolysis kraft pulp using 1,5-diazabicyclo[4.3.0]non-5-enium acetate ([DBNH]OAc) [72–74]. The regenerated Ioncell® fibers have a cellulose II structure (crystallite size ~ 3 nm) with considerable fractions of amorphous domains (crystallinity~50%) and highly oriented voids (between 0.05% and 1% of the total volume) [75]. The fibers were spun at draw ratio six (ratio of take-up to extrusion velocities) and their diameter was close to 13 µm. The fibers dry matter content was 95.7 ± 0.2 wt%. For more information on the Ioncell® fibers and process, the reader can refer to the related literature. The starting material was chosen in context of our groups ongoing research effort concerning the carbonization behavior of different Ioncell® fibers. To cross validate some of the results further measurements with Avicel® PH-101 microcrystalline cellulose as well studied model substance and commercially available levoglucosan ($>$ 99%; Sigma Aldrich) were conducted [76].

2.2. Preparation of heat-treated cellulose samples

About 100 – 150 mg of eight cm length Ioncell® cellulose fibers were distributed evenly in a ceramic boat and heated in a tubular furnace (Nabertherm RHTH 80–300/16, Germany) under 120 L/h of N_2 flow ($N_2 \geq$ 99,999%) up to a final heat treatment temperature (HTT) of 150 °C, 200 °C, 225 °C or 250 °C, and kept for 1 h, 6 h or 11 h. Complementary, Avicel® PH-101 microcrystalline cellulose was treated at the same temperatures for 1 h each. The heating rate was maintained at 5 °C/min for all the experiments. After cooling the gravimetric char yield was calculated and the material was stored in sealed plastic recipients for further analysis.

2.3. Simultaneous thermal analysis coupled to mass spectrometry (STA-MS)

The carbonization dynamics of the precursor fibers (PFs) were studied using an Netzsch STA 449 F3 Jupiter & QMS 403 Aëolos Quadro thermal analyzer. The fibers were heated under a helium atmosphere (70 mL/min) from 40 °C up to 150 °C, 200 °C, 225 °C or 250 °C, at a heating rate of 5 °C/min and kept at the final temperature for 11 h. The sample mass was in the range of 3–5 mg to minimize the heat and mass transfer limitations within the sample. Temperature and heat flux calibration were performed using metal standards with known melting temperatures and enthalpies. The mass spectra of the volatile species emitted during the carbonization were measured with an electron-impact (EI) ionization energy of 70 eV, whether in a continuous mode by screening m/z values from 15 to 180, or in multiple ion detection (MID) mode, at $m/z = 18$, 28 and 44, corresponding to H_2O, CO and CO_2. Using different amounts of calcium oxalate monohydrate (~1–30 mg), which stochiometric thermal decomposition can be determined with very good accuracy using thermogravimetry, we could calibrate the H_2O, CO and CO_2 MS signals using the gravimetric data and quantify their amounts during the carbonization of the cellulose fibers, following a procedure similar to the one described by Maciejewski and

Baiker [77]. The linearity of the mass spectrometer signal is not compromised neither by the heating rate nor by the temperature, which makes it suitable to quantify evolved gases regardless of their emission temperature or the carbonization heating rate [77]. Details about the calibration procedure are given in the electronic supporting information (ESI).

2.4. NMR spectroscopy

NMR spectra were recorded with a Bruker Avance III 400 NMR spectrometer or a Bruker Avance NEO 600 NMR spectrometer. For the collection of solution state NMR spectra a protocol initially developed for cellulose nanocrystals utilizing the solubility of cellulosics in [P_{4444}][OAc]:DMSO-d_6 (1:4 wt%) mixtures was applied [69–71]. The used electrolyte was prepared according to published procedures [69]. In contrast to the original protocol a lower cellulose concentration of 2.5 wt% was used in the majority the experiments. This was necessary to avoid problems with the high viscosity of the dissolved samples introduced by the comparable high degree of polymerization (DP) of the Ioncell® starting material. However, the fibers heat treated at 250 °C and the Avicel® PH-101 samples gave low viscosity solutions even at a concentration of 5 wt%. For the preparation of the NMR samples 25 mg or 50 mg of the heat treated fibers were weighed into a 4 mL glass vial, before [P_{4444}][OAc]:DMSO-d_6 (1:4 wt%) was added until a final weight of 1.0 g. The sealed mixture was stirred with a small magnetic stirring bar and heated to 65 °C by means of an oil bath for 16 – 20 h. Thereafter the samples were transferred into standard 4 mm NMR tubes. All samples were characterized at a measuring temperature of 65 °C by 1D ^{1}H and diffusion edited ^{1}H NMR and 2D multiplicity edited ^{1}H–^{13}C HSQC spectra. For qualitative assignment of peaks ^{1}H–^{13}C HMBC experiments were performed on selected samples. Although available, we did not include ^{13}C NMR spectra in our set of experiments, as they showed insufficient resolution in conducted pretrials. The assignment of ^{13}C peaks is thus only based on the ^{1}H–^{13}C HSQC experiments. An anticipated quantitative evaluation of the spectra was hampered by partial insolubility of some samples, the relative low intensities of the signals introduced by heat treatment and significant peak superposition with the cellulose backbone in the quantitative ^{1}H experiment. Thus, only qualitative, and semi-quantitative information could be obtained. All spectra and peak assignments for the constituents of the starting material (see ESI, Cellulose and Xylan; Tables S3 and S4) are listed in the Electronic Supporting Information.

2.5. FTIR spectroscopy

The FTIR spectra of the original and heat-treated cellulose samples were acquired using a Perkin Elmer Spectrum Two FT-IR Spectrometer (United Kingdom) having a $LiTaO_3$ Detector, an equipped with a Specac Quest Attenuated Total Reflection (ATR) diamond accessory. The spectra were background and base line corrected using the manufacturer's software (Spectrum by Perkin Elmer) and normalized by the band intensity at 1020 cm^{-1} (observed and well-defined characteristic C-O skeletal vibration in secondary alcohols) [78–80]. We report the arithmetic mean of three measurements recorded at different spots for every sample. The spectra acquisition required scanning at room temperature 25 times the wavenumber (v) range from 4000 to 500 cm^{-1} (4 cm^{-1} resolution).

2.6. Size-exclusion chromatography

The SEC-MALS/DRI instrument consisted of Dionex Ultimate 3000 HPLC module, Shodex DRI (RI-101) detector, and Viscotek/Malvern SEC/MALS 20 multi-angle light-scattering (MALS) detector. The columns used were Agilent PLgel MIXED-A (x 4). The flow-rate was 0.75 mL/min. The samples were dissolved in eluent (0.9% LiCl in DMAc) using solvent exchange procedure (water/acetone/DMAc). The injection volume was 100 µl. Detector constants (MALS and DRI) were determined using narrow polystyrene sample (M_w = 96,000 g/mol, $Đ$ = 1.04) dissolved in 0.9% LiCl in DMAc. Broad polystyrene sample (M_w = 248,000 g/mol, $Đ$ = 1.73) was used for checking the detector calibration. The $\partial n/\partial c$ value of 0.136 mL/g was used for celluloses in 0.9% LiCl in DMAc [81].

3. Results

3.1. Sample preparation

The yields of heat-treated Ioncell® cellulose fibers are given in Table 1 and illustrated in Fig. S1 as a function of temperature and holding time (see ESI section on cellulose fiber heat-treatment). The mass loss at 150 and 200 °C was minor and similar yields were obtained at both temperatures. We can assume that no chemical reactions involving the release of volatile species took place within this temperature range, as suggested by Scheirs *et al.* [44].

Lower gravimetric yields were obtained at 225 °C (92.4 wt% after 11 h). The yield started to drop significantly at 250 °C and decreased linearly with the holding time (R^2 =0.999) to reach 74.1 wt% after 11 h. This linear dependence of the mass loss on the holding time is in accordance with early studies on cellulose I (cotton and paper) pyrolysis [18]. According to the same study, the gravimetric yield at 250 °C reaches a plateau only after ~ 180 h.

Considering those results, we can categorize the heat-treated fibers according to the temperature range: those obtained at temperatures of 150–200 °C, for which minor mass loss occurred, and those obtained at 225–250 °C, for which the mass loss starts to be significant. The positive influence of the isothermal pretreatment on obtainable char yield was confirmed by thermal analysis. The Ioncell® cellulose fibers formed a higher char yield at 1100 °C after a stepwise heating including a 1 h holding time at 250 °C (similar to **HTT250–1 h**) compared to a reference measurement without holding time (see ESI section on thermal analyses).

3.2. Appearance and Solubility

For all cellulosic materials, the heat treatments led to a visible discoloration from white (start) over slightly yellow (**HTT150**) to brownish (**HTT200** and **HTT225**) and black (**HTT250**). Thus, reactions in connection with the formation of saccharide-based chromophores must occur already at moderate temperatures [82]. However, they were not formed in quantities detectable by any applied analytical technique. Besides that, only slight shrinkage of the fibers after harsher treatments was observed.

In order to perform solution state protocols like NMR and SEC, the analyte must be soluble in the respective [P_{4444}][OAc]:DMSO-d_6 (1:4 wt %) electrolyte or DMAc/LiCl system. In general, a negative influence of exceeded heating can be expected on the solubility of cellulosic

Table 1
Yields of heat treated Ioncell® cellulose fibers as a function of HTT and holding time.

Sample	HTT / °C	Time / h	Yield / wt% (d.b.)
HTT150–1 h	150	1	98.5
HTT150–6 h	150	6	98.7
HTT150–11 h	150	11	96.5
HTT200–1 h	200	1	94.5
HTT200–6 h	200	6	95.4
HTT200–11 h	200	11	97.0
HTT225–1 h	225	1	93.8
HTT225–6 h	225	6	92.5
HTT225–11 h	225	11	92.4
HTT250–1 h	250	1	92.5
HTT250–6 h	250	6	82.8
HTT250–11 h	250	11	74.1

materials in various solvents, owing to hornification and supramolecular rearrangement phenomena as recently observed in heat treated insulator papers [39,83]. For similarly treated cellulose samples even reluctancy towards hydrochloric acid hydrolysis was observed, which was attributed to the partial formation of a "thermostable condensed phase" [50]. In accordance with the literature, we did encounter dissolution problems to different extents in both SEC and NMR sample preparation in the harsher treated samples (**HTT200–11 h**, **HTT225–11 h**, **HTT250**) owing to an inert solid phase. In the NMR investigations, however, for all samples a cellulosic phase was evident in the spectra. Nonetheless, the inaccessibility of the "thermostable condensed phase" to the performed solution state analytics represents a clear blind spot and must be considered in the interpretation of the results. Noteworthy, in the dissolution of the heat treated Ioncell® fibers in the NMR electrolyte, the insoluble phase kept the fibrous shape of the starting material after dissolution. Moreover, in the samples where first signs of an insoluble phase were discernible (*e.g.*, **HTT200–11 h**), the solid residue did not appear as fine particles, as would be expected for a

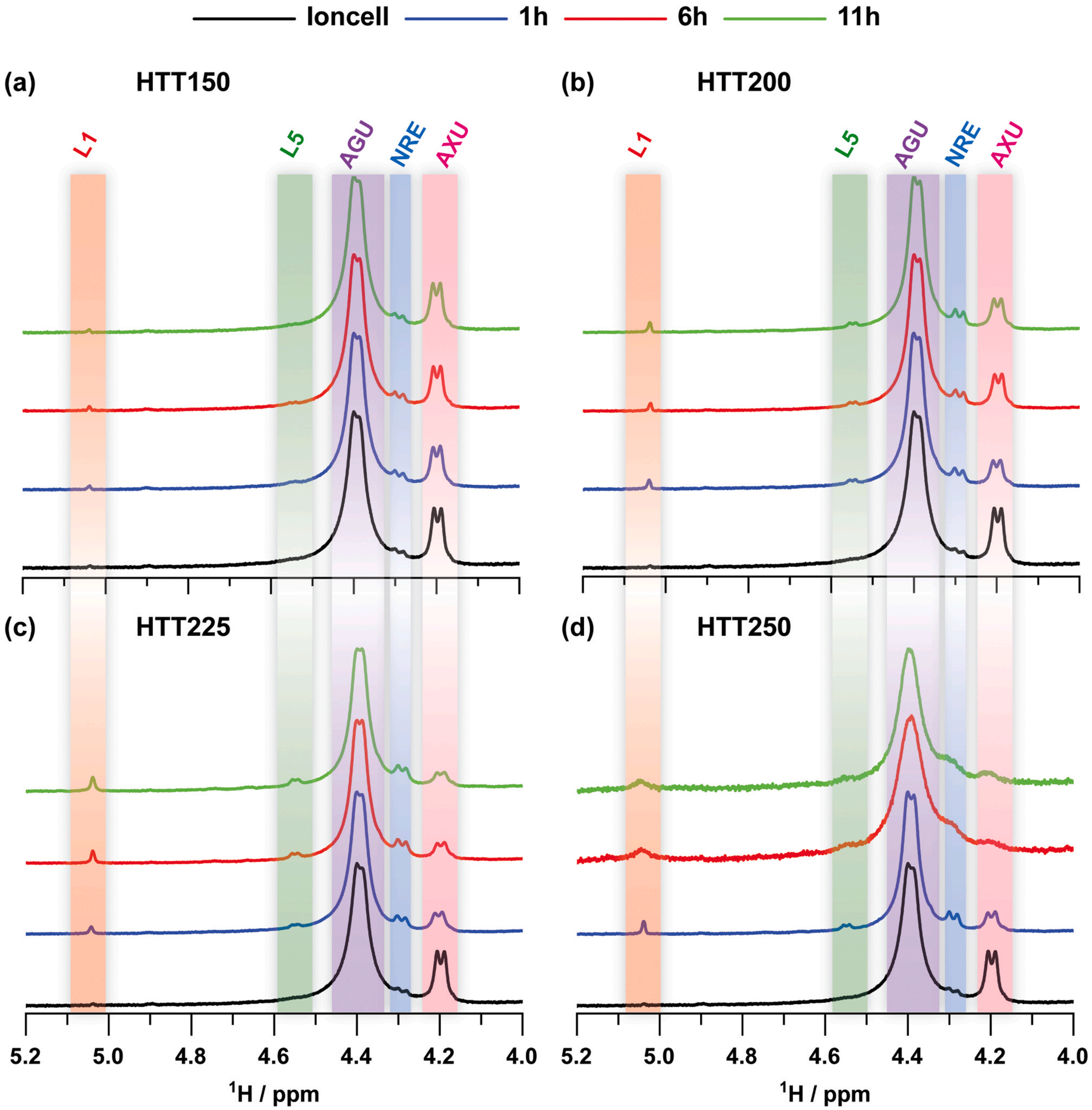

Fig. 1. Comparison of the relative peak intensities of the acetal spectral region of the diffusion edited ^{1}H spectra for the different series of isothermally treated Ioncell® fibers. a) **HTT150**; b) **HTT200**; c) **HTT225**; d) **HTT250**. The spectra show that the chemical changes up to a heat treatment of 225 °C (**HTT225**) are marginal and the materials predominantly consist of AGUs. Two new peaks emerge at 5.05 and 4.55 ppm (**L1** and **L5**, see Fig. 2), which could be assigned to LGA end capped cellulose structures. The relative peak intensities of the non-reducing ends (NREs; see Table S3) increase while no resonances of reducing end groups become visible. This supports the depolymerization of the cellulose backbone under formation of LGA structures. Additionally, the relative intensities of the xylan moieties decrease owing to the reduced thermal stability of the hemicelluloses (AXU; see Table S4). After prolonged treatment at 250 °C (**d**) the accumulation of an insoluble "thermostable condensed phase" in the samples led to problems in the NMR measurements causing badly resolved spectra. Nonetheless, even after 11 h at 250 °C the samples still had a measurable cellulosic fraction. All spectra measured using: [P_{4444}][OAc]:DMSO-d_6 1:4 wt%, 65 °C, 2.5 wt%, 400 MHz. Full spectra are shown in the ESI.

random formation. Instead, full segments of fibers became insoluble. The formation of the so called "thermostable condensed phase" was first described by Pastorova *et al.*, who attributed it to the formation of a "new polymer" [35,50]. Thermal auto-crosslinking of cellulose was often discussed in the literature as having an influence on the progress of the pyrolysis and proposed to occur following different mechanisms [49]. Such thermal cross-linked structures are long known and were initially postulated by Madorsky [84] and later confirmed by Kilzer and Broido [85], who also connected them with increased char yields. However, based on the literature reports we are not certain, if the "thermally crosslinked structures" predominantly postulated to keep their polysaccharidic nature and the "thermostable condensed phase" proposed as a "new polymer" describe the same material or must be treated as separate or subsequent intermediates.

3.2.1. Solution state NMR spectroscopy

For the solution state NMR study, twelve heat treated fibers (see Table 1) and four MCC samples were screened for new functionalities in the bulk material, by comparison with the starting cellulose materials. Thereby, in the heat treatments up to 225 °C even for extended periods of time the differences in the spectra compared to the starting material were rather small. Also, no complete depolymerization to very low molecular weight tar fractions was observed. Only in the diffusion edited ^{1}H spectra, in which the resolution of minor constituents is artificially enhanced [69], additional peaks in the acetal region (approx. 4–5.5 ppm) were visible (see Fig. 1). However, the functionalities were present in low quantities in these samples and did not show clearly discernible signals *e.g.*, in the conducted ^{1}H–^{13}C HSQC experiments. As the applied diffusion editing filters out low molecular weight constituents, the signals can be assigned to transformations on the polymeric chain. There were no signs for either carbonyl or alkene moieties in the dissolved polysaccharidic fractions even after treatment at 250 °C. Furthermore, no signs for degradation to low molecular compounds were apparent in the quantitative ^{1}H or HSQC spectra. These could be expected especially for the postulated keto-anhydroglucose structures, owing to beta-elimination in the alkaline acetate-based NMR electrolyte [86]. Similar degradation phenomena in the NMR solvent were recently reported for periodate oxidized cellulose [70,87]. Given that the employed electrolyte was applicable to a variety of different oxidized cellulosics the dissolution or degradation of the structures proposed by Tang and Bacon can be expected [70,71]. As their presence could not be evidenced, this strongly disfavors their formation in significant quantities in the investigated low temperature range in the cellulose bulk material [38]. Additionally, no signs of degradation or leaching of low molecular compounds (*e.g.*, oligosaccharides, chromophores, aromatics) of the insoluble phase was observed even in the long-time treated samples and considering the harsh dissolution conditions (stirring in [P$_{4444}$][OAc]:DMSO-d_6 (1:4 wt%) at 65 °C for 16–20 h). Notably, low molecular weight compounds were extracted, for example with water [58], and investigated by generally more sensitive chromatography tools. Thus, while they are likewise present, peak superpositions or their low quantities prevented a detection with the applied NMR technique.

In the fiber sample treated for 1 h at 250 °C, the soluble fraction gave very low viscosity solutions, allowing to increase the measuring concentration to 5 wt%. A small portion of "thermostable condensed phase" was already formed leading to particles in the NMR tube. While these are known to affect the measurement, *e.g.*, by impairing the line shaping, the sample still gave very well resolved spectra with high peak intensities. However, in the samples kept at 250 °C for longer periods (**HTT250–6 h** and **HTT250–11 h**), the solid fractions became problematic and led to broad and poorly resolved peaks (see Fig. 1**d** and ESI). Additionally, smaller peaks in the aliphatic region (2.02 and *eg.,*1.24 ppm) emerged in the diffusion edited spectra along with the occurrence of insoluble material. Nonetheless, the spectra evidenced the presence of significant amounts of polysaccharidic fractions even after treatment at 250 °C for 11 h.

In the ^{1}H–^{13}C HSQC spectrum of **HTT250–1h** the peaks in the acetal region (^{1}H = 5.05 and 4.55 ppm) – the same as observed in the resolution enhanced diffusion edited samples in the milder treated samples – showed clear resonances and could be assigned. ^{1}H–^{13}C HMBC spectroscopic analysis of the sample and an overlay with the HSQC spectrum also allowed to connect the observed peaks to a full spin system (Fig. 2). Owing to the strongly reduced DP of the soluble fraction, the HMBC spectrum was well resolved and showed additional interactions of the cellulose backbone compared to the starting material. The most pronounced signal in the acetal region (^{1}H = 5.05 ppm) exhibited clear $^2J_{C\text{-}H}$ and $^3J_{C\text{-}H}$ couplings, partly extending into the polysaccharide backbone region. The evident spin system (Fig. 2) could be assigned to a levoglucosan moiety, and the respective peaks (**L1**-**L6**) are listed in Table 2. Measurements of commercially obtained LGA in both DMSO-d_6 and the [P$_{4444}$][OAc]:DMSO-d_6 (1:4 wt%) electrolyte were performed for comparison and gave spectra with similar shifts as in the heat-treated samples (see ESI Figs. S21-**25**). Further spectroscopic evidence for a LGA unit can be found in the same peak splitting of the diastereotopic hydrogens of the **L6** -CH$_2$ moiety. The observed small aberration in shift values is suspected to be a consequence of the different molecular connectivity at **L4** owing to the bond with the cellulose backbone, which is further evidenced by a $^3J_{C\text{-}H}$ coupling reaching from **L4** over the glycosidic bond to an acetal carbon of the cellulose backbone (Fig. 2 and Table 2).

Levoglucosan can only be present at the reducing end groups (REGs) of the cellulose chains. It is formed either through dehydration of the initially present REGs or transglycosylation along the cellulose backbone. In addition to the markably lower viscosities of the dissolved samples treated at higher temperatures (**HTT250**), depolymerization following isomerization of the AGUs leading to LGA structures is supported by the more pronounced intensity of the **C1** resonance (^{1}H = 4.30 / ^{13}C =102.6 ppm) of the non-reducing end (NRE) with the concomitant absence of signals for REGs (see Fig. 1) [69–71]. Comparing the relative intensities of the **L1** peaks for the different experiments shows that at 150 °C only a small amount of LGA structures is formed even after 11 h (Fig. 1a). The relative intensities for the samples treated at 200 °C, 225 °C and sample **HTT250–1 h** become more pronounced, however, there is no sign that the amount of LGA structures increases significantly either by using higher temperatures or prolonged holding times (Fig. 1b-d). Instead, the intensities remain almost constant. This might be a consequence of subsequent cross-linking reactions of the LGA moieties resulting in steady state-like equilibrium. It is also possible that only parts of the macromolecular cellulose structure, *e.g.*, the amorphous regions, undergo the partial depolymerization, while other, more crystalline areas remain stable.

The additional peaks in the aliphatic region of the samples treated under harsher conditions (see spectral catalogue in ESI) were more difficult to assign, owing to strong superposition with the signals of the [P$_{4444}$][OAc] electrolyte, especially in the 2D NMR spectra. Thus, assignments had to rely on the shifts in the diffusion edited ^{1}H experiment. The peak observed at 2.02 ppm is characteristic for cellulose acetate and was recently assigned to a stereoselective acetylation at the **C6** position of the cellulose backbone [88,89]. In this study the cellulose acetate most likely is formed during dissolution through a side reaction of the acetate anion in the electrolyte with a generated unstable or reactive intermediate in the cellulosic materials. We considered a reaction of the LGA end-capped moiety as the origin of the signal, but the control experiment with commercial levoglucosan did not show such an acetate formation in the electrolyte solution under the applied dissolution and measuring conditions (65 °C, 16 h; see ESI Figs. S24–25). Also, 1, 2-anhydroglucose which was postulated as precursor in the formation of levoglucosan [90] could be excluded as possible source of the signal at 2.02 ppm, as opening of the epoxide functionality would result in modifications either on **C1** or **C2** of the moiety with expected shift values below 2 ppm. In conclusion, we admittedly cannot identify the exact nature of the intermediate responsible for the **C6**-acetate peak.

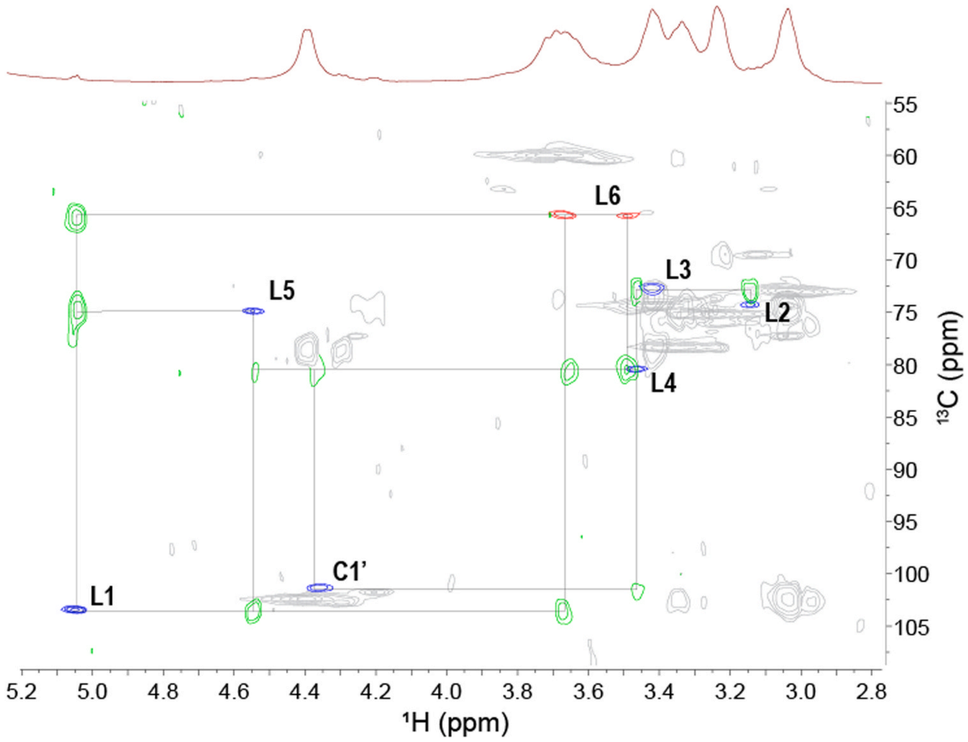

Fig. 2. Zoom into the polysaccharide region of an overlay of a multiplicity edited ^{1}H–^{13}C HSQC (CH and CH_3 = blue; CH_2 = red) and a ^{1}H–^{13}C HMBC (green) spectrum for an Ioncell® fiber treated at 250 °C for 1 h (**HTT250–1 h**; measuring concentration = 5 wt%) Only peaks of the LGA end capped cellulose moieties are highlighted (**L1**-**L6**), while the residual cellulose, hemicellulose and unassigned peaks are shown in grey (see ESI Tables S3 and S4). The signals and multiple bond correlations are in accordance with the LGA structure (see ESI Figs. S21-25). A $^{3}J_{C\text{-}H}$ coupling between **L4** and an acetal cellulose peak (**C1'**) proves the attachment to the cellulose backbone. Both spectra obtained using: $[P_{4444}][OAc]$:DMSO-d_6 1:4 wt%, 65 °C, 400 MHz ^{1}H frequency. Diffusion edited ^{1}H spectrum shown on top.

Table 2
Peak assignment for LGA end capped cellulose resonances according to the ^{1}H–^{13}C HSQC spectrum of sample **HTT250–1 h** ($[P_{4444}][OAc]$: DMSO-d_6 (1:4 wt%); 65 °C; measuring concentration = 5 wt%).

Structure:	Atom Nr.:	^{1}H / ppm	^{13}C / ppm
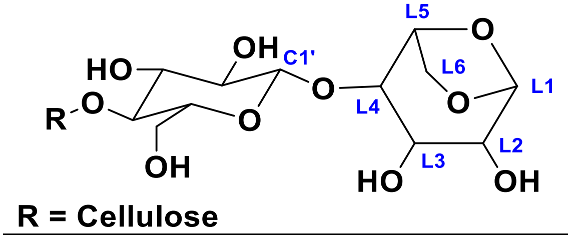	**L1**	5.05	103.4
	L2[a]	3.14	74.2
	L3[a]	3.42	72.6
	L4	3.47	80.4
	L5	4.55	74.9
	L6	3.67 / 3.49	65.7
	C1'[b]	4.36	101.3

[a] owing to intensive peak overlap in the spectral region, the actual shifts might vary
[b] resonance of the cellulose AGU neighboring the levoglucosan end cap

Aliphatic signals below 2 ppm – most pronounced at 1.24 ppm – in the diffusion edited ^{1}H experiments could not be assigned at all, as they did not exhibit significant peaks in the other conducted NMR experiments and heavily superimposed with the residual $[P_{4444}][OAc]$ resonances. However, the observed shifts are not in accordance with alpha carbonyl protons as expected for the postulated dehydrated carbonyl structures. Based on their shifts the peaks should be caused by simple alkyl chains, not connected to oxygen. However, it is unclear how these moieties would form in the polymer fractions at the investigated temperature ranges. The signals could as well be artifacts from insufficient diffusion editing or stem from leaching of the residual suspended particles. Noteworthy, peaks or plateaus in the aliphatic region were also observed in solid state ^{13}C NMR investigations of cellulose treated at 300–400 °C [42].

Besides the signals of the polymeric fractions no evidence for low molecular mass compounds associated with the tar forming reaction pathway were obtained. This is ascribable to the presumably small amount of formed tar fractions at the investigated temperature, superposition with the more pronounced polymeric peaks and the significantly lower resolution of the applied method compared to, *e.g.*, the GC-MS protocols commonly used for the investigation thereof. Importantly, there was also no sign of monomeric levoglucosan in considerable quantities (compare peak differences of Fig. 2 with Figs. S24–25 in ESI) but clear evidence of cellulose bound LGA-structures.

On a qualitative basis the used fibers were comparably stable towards both, the investigated heat treatments, and the conducted sample preparation. However, there was a clear difference between the stability of the cellulose and hemicellulose constituents of the fibers towards heating. The peaks of the anhydroxylan units (AXU, see ESI Table S4) disappeared during prolonged treatment at 250 °C (Fig. 1d). The reduced thermal stability of hemicelluloses compared to cellulose is well known [91–93].

Noteworthy, in the **HTT250–1 h** sample also a relatively strong, characteristic peak emerged in the HSQC spectra (CH or CH_3 at ^{1}H = 4.26 / ^{13}C = 77.3 ppm), which was connected to various peaks in the polysaccharide region through HMBC interactions. We suspect this peak might stem from a crosslinked structure. However, owing to strong superpositions by the other constituents we did not succeed in elucidating the structure responsible for this spin system.

To cross validate the results, a comparative NMR study was conducted on similarly heat treated Avicel® PH-101 (see ESI Figs. S62–73), as a well understood cellulose model substance [76]. Only samples treated for 1 h in the four respective temperature steps were prepared, as the longer lasting experiments did not introduce significant chemical changes in the fiber substrate. On a qualitative basis the results were in accordance with the fiber measurements and only the formation of LGA end capping without carbonyl formation was observed. However, the highly crystalline cellulose I material proved to be more thermally stable than the fibers, consisting of cellulose II with a higher share of amorphous regions. Thus, no significant formation of an insoluble thermostable phase at 250 °C was observed and the depolymerization of the soluble fractions was negligible. While the spectra were recorded on a spectrometer with a higher magnetic field (600 MHz *vs* 400 MHz), the investigated dissolved NMR samples did not give additional information on the chemical composition, owing to low relative peak intensities and higher viscosity. Also, the still visible hemicellulose resonances rendered Avicel® PH-101 as a non-ideal model compound for the solution state NMR investigations (see ESI Fig. S64).

3.3. *Thermal analysis*

The STA-MS experiments offered insights on the dynamics of mass loss and gas emission during the heat-treatment. The mass loss combined with H_2O and CO_2 emission profiles during heat treatment experiments at 200 and 250 °C are shown in Fig. 3. The results confirm the low mass loss at 200 °C, which was accompanied by a sharp release of water during the drying stage at 105 °C, and a subsequent and a surprising cyclic water release once the 200 °C plateau was reached. According to the published literature, the temperature of 200 °C seems to be the minimum temperature at which water can evolve from chemical processes during cellulose pyrolysis [44]. However, it was postulated that the water emitted at the 200 °C plateau corresponds to a structural or bound water, which is more difficult to remove thermally from the cellulose structure, in comparison with more loosely bound excess water [94]. The minor amount of CO_2 corresponding to a small and noisy emission peak close to 200 °C, can result from the decomposition of the less thermally stable residual hemicelluloses.

The mass loss rate increased significantly during the 250 °C experiments due to the exponential dependence of the reaction rate on temperature. The water and carbon dioxide emission profiles followed closely the mass loss rate curve (see ESI, section on thermal analysis). The gravimetric mass loss in the 200 °C experiment matched well with the mass of emitted H_2O and CO_2 quantified by mass spectrometry. In the 250 °C experiment, the gravimetric mass loss (21.2 wt%) was higher than the mass of H_2O and CO_2, which represented respectively 6.7 wt% and 4.4 wt% of the initial cellulose mass and a bit more than 50% of the overall gravimetric mass loss. An overview of reactions leading to the chemical formation of water from cellulose is given in a comprehensive review by Scheirs *et al.* [44]. The residual mass loss can be ascribed to evaporation of low molecular weight organic compounds expulsed following tar forming or fragmentation reactions.

The very close correspondence of the H_2O and CO_2 emission profiles with the peak of mass loss rate suggest that they are the products of fast dehydration and decarboxylating secondary reactions with respect to the main controlling step of depolymerization by LGA formation. Cellulose pyrolysis thermograms are well described by a first order rate equation with a high activation energy (close to 200 kJ/mol) corresponding to the transglycosylation step [26]. A similar model is shown in the ESI and gives a pre-exponential factor and an activation energy of $3.8\ 10^{17}\ s^{-1}$ and 234 kJ/mol, respectively. Such a high activation energy cannot be attributed to dehydration or decarboxylation reactions. According to the first-order global kinetic model describing cellulose pyrolysis (see ESI), at a constant temperature, the mass loss rate divided by the remaining mass at the time *t* corresponds to the rate constant. Assuming the elimination of LGA ends occurs with the same rate of transglycosylation, we can estimate an average time – expressed as the inverse of the rate constant – which LGA spends in the cellulose matrix in a linked form [20]. The time corresponds to ~ 50,000 h and ~ 170 h, respectively at 200 °C and 250 °C. This explains the accumulation of LGA end capped structures in the materials and their detection in the NMR spectra from a thermodynamic point of view.

3.3.1. *FTIR spectroscopy*

FTIR spectroscopy was applied to monitor the chemical and structural changes in the original and heat-treated cellulose fibers. The FTIR

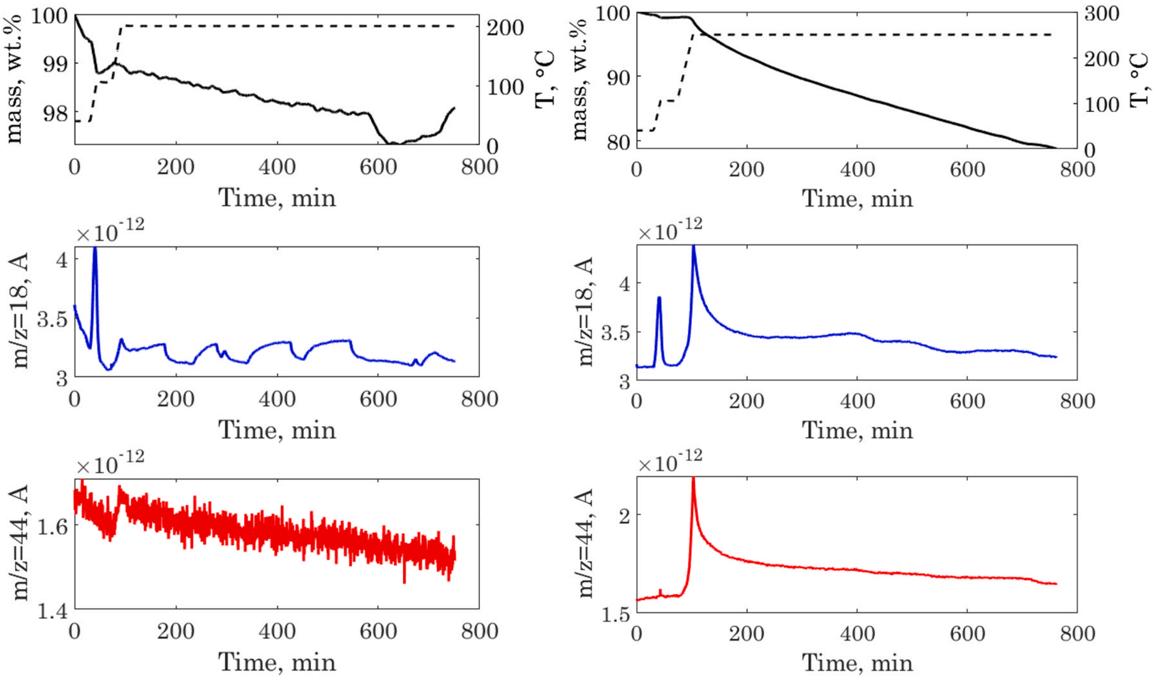

Fig. 3. Mass loss, H_2O and CO_2 emission profiles as a function of time during the heat-treatment of Ioncell® cellulose fibers at 200 °C (left) and 250 °C (right).

spectra of the original and heat-treated Ioncell® cellulose fibers are shown in Figs. S10-S13 in the **ESI**. The FTIR spectrum of the original fibers contains several bands which are characteristic of the molecular vibrations in cellulose II structures [95,96].

The spectra of the original and heat-treated fibers at 150 – 200 °C are essentially the same, regardless of the holding time. Slightly lower OH stretching band intensity in fibers treated at **HTT200** may indicate the beginning of dehydration, or the weakening and rupture of hydrogen bonds due to the thermal stress [97], especially at the highest holding time in **HTT200–11 h**.

The intensity of the band at ~990 cm^{-1}, which is assigned to C-O skeletal vibration in secondary alcohols, decreased at 225 °C and is connected to the occurrence of dehydration reactions, as suggested by Pastorova *et al.* [35]. However, it remains unclear to us why this band intensity increased again in **HTT250–1 h** and decreased for longer holding times.

IR absorption at frequencies of ~1610 and ~1710 cm^{-1}, corresponding respectively to the stretching vibrations of C=C and C=O bonds, increased markedly in **HTT250–6 h** and **HTT250–11 h**. They are associated with the formation of C=C bonds and carbonyl structures. The carbonyl groups might participate in a variety of thermal degradation reactions also involving carboxyl groups, which can give rise to carbon monoxide and carbon dioxide, as observed in our STA experiments at 250 °C.

Decoupling the contribution of the C=C stretching from the O-H bending vibrations (~1640 cm^{-1}) remained challenging as their absorption frequency regions overlap. However, the occurrence of an O-H stretching band in the 3000–3700 cm^{-1} region suggest that the O-H bending vibrations still contribute to the absorbed intensity in the 1500–1700 cm^{-1} region. Besides the marked changes in the C=O and C=C absorption regions, the small changes in the C-O stretching in the pyranose ring at ~1110 cm^{-1} and C-O-C skeletal vibrations at 1020 cm^{-1} suggest that the pyranose structures of the cellulose chains remain essentially unaltered.

Altogether, FTIR spectroscopy indicated that the dehydration reactions of Ioncell® cellulose II fibers start in the temperature range of 225 – 250 °C and become significant at 250 °C for holding times higher than 1 h. It seems that except for the samples prepared at 250 °C, the lower temperature samples underwent mainly DP reduction reactions and less extensively dehydration reactions.

Concerning the MCC samples (see Fig. S14), except some decrease in the OH stretching vibration band intensity, the spectra of MCC samples treated at the four temperatures for 1 h are similar. This greater similarity of the spectra can be explained by the higher thermal stability of MCC due to its cellulose I structure.

3.3.2. *Size-exclusion chromatography*

Regenerated cellulose fibers represent a challenging analyte for SEC analysis in general, which is expectedly further aggravated by the performed heat treatments. Especially when samples were treated under harsher conditions and a “thermostable condensed phase” was formed, problems with partial insolubility were observed. While the obtained SEC data and the thereof derived molar mass averages are thus knowingly compromised and should be interpreted with care, comparison of the soluble fractions still allowed for insights into the depolymerization and subsequent crosslinking reactions. Molar-mass averages (M_w and M_n) and dispersities ($Đ$) for heat-treated Ioncell® fibers are listed in Table 3. Already with moderate heat treatment at 150 °C the molar mass increased, indicating cross-linking. Usually, low temperature heat pretreatments were related to depolymerization reactions to a level-off DP [49]. However, unexpected repolymerization was also observed in a thorough SEC study on insulator papers aged at 170 °C for extended periods [83]. In our experiments the presumed onset of re-polymerization was observed at lower temperatures and treatment times. This might be a consequence of the lower thermal stability of the regenerated cellulose II fiber, compared to the cellulose I insulator papers used by Jusner *et al.* [83]. Another indication for competing depolymerization and repolymerization reactions can be found in the increasing dispersities for heat-treated samples compared with the reference fiber (Table 3). Furthermore, the molar masses for samples heat-treated at higher temperatures did not show a clear trend for either preferred depolymerization or cross-linking over the investigated temperature range.

Table 3
Molar mass averages (M_w, weight-average molar mass; M_n, number-average molar mass) and dispersities ($Đ$) for heat-treated cellulose samples.

HTT / °C	M_w / kDa	M_n / kDa	$Đ$
Ref.	155	63	2.5
150	265	73	3.6
200	77	12	6.4
230	222	38	5.9
250	51	6	8.4

Evidence on the cross-linked structures could also be obtained from the conformation plots (double logarithmic plot of radius of gyration and molar mass) which are overlaid in Fig. 4. The relationship between radius and molar mass gives information on polymer architecture [98]. The slope of the fitted straight line of around 0.33 indicates the presence of compact and/or branched structures, the slope of around 0.5 is typical for random coil polymers in a good solvent, and slope of around 1 indicates the presence of extended rod-like structures [99]. In general, for linear polymers such as for cellulose, radius of gyration increases with increasing molar mass. This is the case for the reference fiber. Also, the slope of the conformation plot for the reference fiber (covering the molar mass range from around tens to a couple of hundred kDa) is in the range of a typical random coil polysaccharide (0.55). This is clearly not the case for the heat-treated samples for which the slope in this same molar mass region is significantly lower. This indicates the presence of branched, cross-linked structures. Again, similar yet less pronounced cross linking in the conformation plots was observed in the aged insulator papers [83]. The slope for the fiber treated at 200 °C (0.26) was higher compared to the slopes of the other heat-treated samples (close to 0). At this temperature, the depolymerized fragments seem to be more linear compared to the fragments released at the higher temperature of 250 °C. The difference between the slopes is not that substantial in the high-molar-mass region.

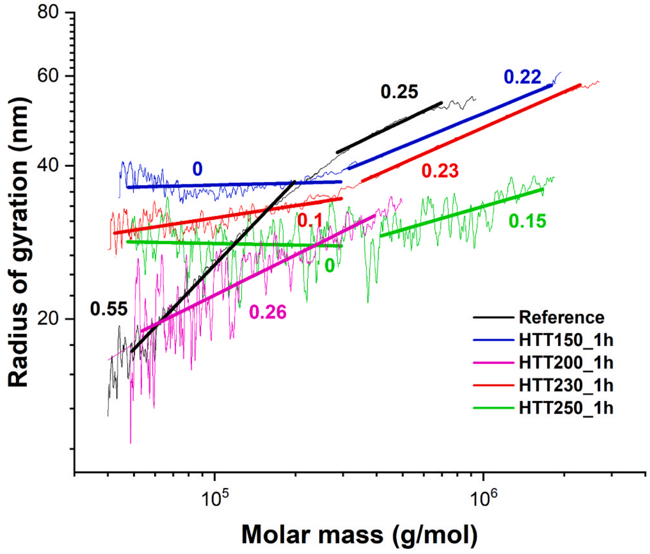

Fig. 4. Conformation plots with linear fitting and slopes of the fitted data for heat-treated samples and the untreated reference.

3.4. Discussion

The conducted experiments allowed for additional insights into the chemical and structural transformations during the early stages of cellulose pyrolysis at temperatures below 250 °C. Foremost, by utilizing solution state NMR it was possible to unequivocally prove the occurrence of LGA end capped cellulose structures as first and dominant intermediate in the bulk material. In accordance with previous *in-silicio* studies [59], we could experimentally validate that the formation of LGA structures first occurred at the reducing end groups. At temperatures around 200 – 250 °C further LGA moieties were formed through intramolecular transglycosylation reactions leading to chain scissions. As the LGA groups were bound to cellulose and no signs of free, monomeric LGA (compare Fig. 2 and Figs. S24-25) were evident, we conclude that the scission selectively at the ends leading to “unzipping” of the polymer does not occur in significant quantities in the investigated temperature ranges. The presence of LGA bound to cellulose as compared to the presence of monomeric LGA, also agrees with kinetic models suggesting that LGA exists predominantly bound to cellulose and the formation of LGA end capped structures is the rate-limiting step [20]. Up to a temperature of 225 °C the investigated samples proved to be fully soluble in the NMR electrolyte and did not show any significant chemical transformations, except for the presence of small quantities of LGA end capped structures only visible in the diffusion edited ^{1}H spectra. This can be a consequence of the dehydration of pre-existing reducing end groups (REGs) or REGs formed through often-observed thermal depolymerization in the amorphous regions. In the harsher treated cellulosics (**HTT250–1 h**) two distinguishable fractions were observed: An easily soluble fraction consisting of very low DP LGA-end capped cellulosic structures, characterized by low viscosity after dissolution and high end-group peak intensities in the NMR spectra; and a second completely insoluble and inert fraction, dark-brown to black in its appearance. This observation is in line with previous reports, where the latter fraction was termed as “thermostable condensed phase” and even resisted hydrochloric acid hydrolysis [35,50].

There were no signs for either alkene or carbonyl functionalities in the NMR spectra up to 225 °C and in the soluble fractions at 250 °C. However, clear vibrations for these moieties were discernible in the FTIR spectra for the samples treated at 250 °C. As the vibrations only appeared in connection with the occurrence of the insoluble fraction, we emphasize that the associated dehydration reactions predominantly occur in the insoluble phase. Noteworthy, a discrepancy between solid state NMR and IR spectroscopy was also observed previously, where no significant carbonyl peak intensities were observed in ^{13}C NMR spectra of microcrystalline cellulose heat treated at 250 °C, while the bands were clearly present in the IR spectra. Only after treatment at 270 °C carbonyls were discernible both in solid state NMR and IR [35].

Thus, the AGU repeating units proved to be more stable towards dehydration reactions than in other postulated mechanisms, *e.g.*, from Tang and Bacon [38], where the onset of the reaction is set to 150 °C. Instead, up to at least 225 °C no serious dehydration from the cellulose backbone could be evidenced, even while working with less thermally stable cellulose II fibers. In line with the conclusions of Antal [49] results favoring the importance of depolymerization and cross-linking phenomena of the polysaccharides in the respective temperature range were obtained. While also suffering from partial solubility issues in the DMAc / LiCl system, the SEC results hinted towards strong structural changes in the soluble fractions, shown as the high molar mass dispersities and crosslinking.

The herein used experimental setup proved to be insufficient to get further insights into the cross-linked fractions by NMR spectroscopy. Given the evidenced presence of LGA structures and the similarities between the products of levoglucosan and cellulose carbonization, [63] there are probably some similarities in their thermo-induced bond formation as well [60–62]. The results of LGA thermal polymerization hinted towards a cationic polymerization with an autocatalytic behavior, which adds another layer of complexity to the problem [62]. However, the carbonization of pure levoglucosan did not show significantly higher char yields than cellulose [55]. Thus, the operative reactions must be more complex and include synergistic effects of levoglucosan and anhydroglucose structures. The remarkably high char yields obtained from a LGA end capped disaccharide structure (maltosan) would support this claim [55]. Presumably, the presence of a more reactive primary alcohol structure at C6 is important for the crosslinking [61]. However, also other crosslinking reactions, like transetherfications were reported in heat treated celluloses and might contribute to the overall reaction scheme.

Based on our results and literature reports LGA containing structures thus very likely occur and participate in the char forming pyrolysis pathway and not only in the tar formation. However, as was pointed out by Kawamoto in his seminal review on the operative chemistry of cellulose pyrolysis [100], the crosslinking of LGA moieties represents a reversible reaction and the formed structures do not offer a viable explanation for the subsequent dehydration reactions. Additionally, the SEC results indicated that significant crosslinking already occurred at temperatures (150 – 225 °C; or 170 °C [83]) not having a sizeable effect on overall char yields [43]. Thus, while the crosslinking of LGA structures likely influences the carbonization process by partly reversing the unzipping reactions and “capturing” LGA moieties in the solid fractions, we are skeptical that it is directly responsible for the observed higher char yields. Instead, we surmise the thermal cross-linking only enables the subsequent dehydration by introducing different glycosidic bonds and loosening or breaking-up the rigid H-bonding patterns in the crystalline areas, associated with the high thermal stability of cellulose compared to chemically similar polysaccharides [59,100]. This might lead to a partial transformation to pyrodextrin-like compounds which are known to be less thermally stable [49].

Regarding the operative dehydration mechanism, no structures for carbonization intermediates could be directly evidenced in this study. Given the occurrence of carbonyl and alkene bands in the FTIR of harsher treated samples in connection with the detection of water in the STA-MS experiments, reactions leading to the expulsion of water from the solid residue occurred at least in the range of 225–250 °C. This coincided with the formation of an insoluble and inert phase, previously described as “thermostable condensed phase”. To the best of our knowledge the composition of this material was only investigated once [35], and the transformation of cellulose to a “new polymer” with furanoid skeletons, hydroxyaromatic skeletons, unsaturated hydrocarbon chains, carbonyl and carboxylate functionalities was proposed. Based on our NMR study it seems likely that dehydration reactions lead to its formation and that the subsequent reactions at higher temperatures – ultimately resulting in the formation of char – occur in this insoluble phase. It should be noted that the herein applied NMR electrolyte was applicable for a variety of polysaccharides and was more specifically used to analyze different oxidized celluloses [69–71]. Structures formed from simple dehydration of the AGUs as proposed in literature should have shown at least partial solubility or degradation peaks owing to beta elimination reactions [86]. Furthermore, it seems unlikely that simply oxidized structures would have withstood the acid hydrolysis protocol as reported in literature [50]. These observations contrast with mechanistic proposals where simple dehydration from the cellulose backbone is proposed [38]. While we could not further add to the elucidation of the chemical composition of the “thermostable condensed phase” in this study, we support the claim of Pastorova *et al.* that it is formed following more complex transformations. Importantly, this insoluble phase should be differentiated from thermally cross-linked polysaccharides formed during earlier cellulose heat treatment, which showed at least partial solubility in the NMR and SEC electrolytes. These polysaccharidic fractions represent a separate intermediate, which can pyrolyze both following the carbonization pathway after dehydration and transformation to the “thermostable condensed phase” or following the tar forming pathway after “unzipping” to volatile LGA at higher temperatures. We surmise that only the “thermostable condensed phase” represents an important intermediate of the char forming pyrolysis pathway.

Overall, this study also once again highlighted the analytical difficulties connected with the study of the chemistry of cellulose heat treatments. Our approach allowed to investigate the formed chemical structures with so far not attainable resolution. Nonetheless, it suffered from analytical blind spots introduced by partial (in)solubility, thus providing only another piece of the complete picture. Also, we did not consider several factors in our experimental design, like the supramolecular structural changes [39], the consequences of the non-homogenous progress of the transformations caused by heat transfer limitations [59] or the occurrence of possibly catalytically active secondary reactions [20,27,28] in this work. Likewise, they all have a considerable influence on the overall course of the reaction in the investigated temperature range. In general, given the already exhaustive – and partly contradicting – literature concerning the investigated topic a holistic research approach considering all already reported contributing factors seems hardly possible [23,44,49,100].

4. Conclusions and outlook

Application of state-of-the-art solution state analytical techniques allowed to reinvestigate several aspects of the chemistry of low temperature pretreatment of cellulosic fibers. Solution state NMR evidenced the predominant formation of LGA moieties at the reducing ends of cellulose fragments as first step of the occurring transformations. Also, the general onset of the reactions was found to be higher than reported in literature. Up to a temperature of 225 °C no signs for newly formed chemical functionalities were discernible, except for LGA moieties caused by intramolecular transglycosylation and the transformation of existing reducing end groups. In the SEC experiments both thermal chain scission and cross-linking was evident in the conformation plots and the high dispersity of molar mass distributions. The findings are in line with several studies highlighting the importance of reducing ends and LGA moieties during cellulose carbonization. However, while these observed reactions likely participate in the overall carbonization scheme, they do not offer a viable explanation for the occurring dehydration mechanisms.

Instead, our reinvestigation hinted towards the importance of an additional phase as a likely intermediate in the dehydration and subsequent carbonization pathway. This previously described “thermostable condensed phase” exhibited an interestingly recalcitrant dissolution behavior and was so far not extensively examined. Our future investigations will focus on the formation and chemistry of this material, to obtain further insights into the reaction mechanisms operative during cellulose dehydration.

The potential of the applied solution state NMR protocol was demonstrated but not yet fully exploited in this study. The Ioncell® fibers predominantly used as starting material – although closer to the actual industrial application of carbon fiber production – possessed suboptimal properties for the collection of NMR spectra, owing to comparably high DP and residual hemicellulose content, leading to peak superpositions. Thus, we are optimistic that the utilization of high purity and lower DP cellulose model compounds and higher magnetic field spectrometers can unravel further aspects of cellulose pyrolysis.

CRediT authorship contribution statement

Lukas Fliri: Conceptualization, Methodology, Validation, Formal analysis, Investigation, Visualization, Writing – Original Draft, Writing – Review and Editing. **Chamseddine Guizani**: Conceptualization, Methodology, Validation, Formal analysis, Investigation, Supervision, Writing – Original Draft, Writing - Review & Editing. **Isaac Yair Miranda-Valdez**: Formal analysis, Investigation, Visualization. **Leena Pitkänen**: Validation, Formal analysis, Investigation, Visualization, Writing – Review and Editing. **Michael Hummel**: Supervision, Writing - Review & Editing, Project administration, Funding acquisition.

Declaration of Competing Interest

The authors declare that they have no known competing financial interests or personal relationships that could have appeared to influence the work reported in this paper.

Data availability

The data that support the findings of this study are available from the corresponding authors on reasonable request.

Acknowledgment

The authors gratefully acknowledge funding from the Academy of Finland (Project: 348354). The authors thank Muhammad Awais for help in the visualization of the results.

Appendix A. Supporting information

Supplementary data associated with this article can be found in the online version at doi:10.1016/j.jaap.2023.106153.

References

[1] M.J. Antal, M. Gronli, The art, science, and technology of charcoal production, Ind. Eng. Chem. Res. 42 (8) (2003) 1619–1640, https://doi.org/10.1021/ie0207919.

[2] A.V. Bridgwater, Review of fast pyrolysis of biomass and product upgrading, Biomass-.-. Bioenerg. 38 (2012) 68–94, https://doi.org/10.1016/j.biombioe.2011.01.048.

[3] X. Hu, M. Gholizadeh, Biomass pyrolysis: A review of the process development and challenges from initial researches up to the commercialisation stage, J. Energy Chem. 39 (2019) 109–143, https://doi.org/10.1016/j.jechem.2019.01.024.

[4] M.I. Jahirul, M.G. Rasul, A.A. Chowdhury, N. Ashwath, Biofuels production through biomass pyrolysis-A technological review, Energies 5 (12) (2012) 4952–5001, https://doi.org/10.3390/en5124952.

[5] T. Kan, V. Strezov, T.J. Evans, Lignocellulosic biomass pyrolysis: A review of product properties and effects of pyrolysis parameters, Renew. Sust. Energ. Rev. 57 (2016) 1126–1140, https://doi.org/10.1016/j.rser.2015.12.185.

[6] M.S. Mettler, D.G. Vlachos, P.J. Dauenhauer, Top ten fundamental challenges of biomass pyrolysis for biofuels, Energ, Environ. Sci. 5 (7) (2012) 7797–7809, https://doi.org/10.1039/C2EE21679E.

[7] D. Mohan, C.U. Pittman, P.H. Steele, Pyrolysis of wood/biomass for bio-oil: A critical review, Energ. Fuel 20 (3) (2006) 848–889, https://doi.org/10.1021/ef0502397.

[8] A. Oasmaa, J. Lehto, Y. Solantausta, S. Kallio, Historical review on VTT fast pyrolysis bio-oil production and upgrading, Energ. Fuel 35 (7) (2021) 5683–5695, https://doi.org/10.1021/acs.energyfuels.1c00177.

[9] G. Varhegyi, From "Sirups" to Biocarbons: A 30 Year Research Cooperation for Better Biomass Utilization with Michael J. Antal, Jr, Energ. Fuel 30(10) (2016) 7887–7895, https://doi.org/10.1021/acs.energyfuels.6b00860.

[10] G.Y. Wang, Y.J. Dai, H.P. Yang, Q.G. Xiong, K.G. Wang, J.S. Zhou, Y.C. Li, S. R. Wang, A review of recent advances in biomass pyrolysis, Energ. Fuel 34 (12) (2020) 15557–15578, https://doi.org/10.1021/acs.energyfuels.0c03107.

[11] S.R. Wang, G.X. Dai, H.P. Yang, Z.Y. Luo, Lignocellulosic biomass pyrolysis mechanism: A state-of-the-art review, Prog. Energ. Combust. 62 (2017) 33–86, https://doi.org/10.1016/j.pecs.2017.05.004.

[12] S. Williams, C. Higashi, P. Phothisantikul, S. Van Wesenbeeck, M.J. Antal, The fundamentals of biocarbon formation at elevated pressure: From: 1851 to the 21st century, J. Anal. Appl. Pyrol. 113 (2015) 225–230, https://doi.org/10.1016/j.jaap.2014.12.021.

[13] A. Broido, M.A. Nelson, Char yield on pyrolysis of cellulose, Combust. Flame 24 (2) (1975) 263–268, https://doi.org/10.1016/0010-2180(75)90156-X.

[14] P.H. Brunner, P.V. Roberts, The significance of heating rate on char yield and char properties in the pyrolysis of cellulose, Carbon 18 (3) (1980) 217–224, https://doi.org/10.1016/0008-6223(80)90064-0.

[15] D.F. Arseneau, Competitive reactions in thermal decomposition of cellulose, Can. J. Chem. 49 (4) (1971) 632, https://doi.org/10.1139/v71-101.

[16] A.G.W. Bradbury, Y. Sakai, F. Shafizadeh, Kinetic-model for pyrolysis of cellulose, J. Appl. Polym. Sci. 23 (11) (1979) 3271–3280, https://doi.org/10.1002/app.1979.070231112.

[17] A. Broido, A.C. Javierso.Ac, E.M. Ouano, Barrall, Molecular-weight decrease in early pyrolysis of crystalline and amorphous cellulose, J. Appl. Polym. Sci. 17 (12) (1973) 3627–3635, https://doi.org/10.1002/app.1973.070171207.

[18] A.E. Lipska, W.J. Parker, Kinetics of pyrolysis of cellulose in temperature range 250-300 degrees C, J. Appl. Polym. Sci. 10 (10) (1966) 1439, https://doi.org/10.1002/app.1966.070101005.

[19] A.E. Lipska, F.A. Wodley, Isothermal pyrolysis of cellulose - kinetics and gas chromatographic mass spectrometric analysis of degradation products, J. Appl. Polym. Sci. 13 (5) (1969) 851, https://doi.org/10.1002/app.1969.070130504.

[20] V. Mamleev, S. Bourbigot, M. Le Bras, J. Yvon, The facts and hypotheses relating to the phenomenological model of cellulose pyrolysis Interdependence of the steps, J. Anal. Appl. Pyrol. 84 (1) (2009) 1–17, https://doi.org/10.1016/j.jaap.2008.10.014.

[21] G. Varhegyi, E. Jakab, M.J. Antal, Is the broido-shafizadeh model for cellulose pyrolysis true, Energ. Fuel 8 (6) (1994) 1345–1352, https://doi.org/10.1021/ef00048a025.

[22] C. Serbanescu, Kinetic analysis of cellulose pyrolysis: a short review, Chem. Pap. 68 (7) (2014) 847–860, https://doi.org/10.2478/s11696-013-0529-z.

[23] J. Lede, Cellulose pyrolysis kinetics: An historical review on the existence and role of intermediate active cellulose, J. Anal. Appl. Pyrol. 94 (2012) 17–32, https://doi.org/10.1016/j.jaap.2011.12.019.

[24] J.P. Diebold, A unified, global-model for the pyrolysis of cellulose, BiomassBioenerg. 7 (1–6) (1994) 75–85, https://doi.org/10.1016/0961-9534(94)00039-V.

[25] A.M. Emsley, G.C. Stevens, Kinetics and mechanisms of the low-temperature degradation of cellulose, Cellulose 1 (1) (1994) 26–56, https://doi.org/10.1007/BF00818797.

[26] M. Gronli, M.J. Antal, G. Varhegyi, A round-robin study of cellulose pyrolysis kinetics by thermogravimetry, Ind. Eng. Chem. Res. 38 (6) (1999) 2238–2244, https://doi.org/10.1021/ie980601n.

[27] V. Mamleev, S. Bourbigot, J. Yvon, Kinetic analysis of the thermal decomposition of cellulose: The main step of mass loss, J. Anal. Appl. Pyrol. 80 (1) (2007) 151–165, https://doi.org/10.1016/j.jaap.2007.01.013.

[28] V. Mamleev, S. Bourbigot, J. Yvon, Kinetic analysis of the thermal decomposition of cellulose: The change of the rate limitation, J. Anal. Appl. Pyrol. 80 (1) (2007) 141–150, https://doi.org/10.1016/j.jaap.2007.01.012.

[29] I. Milosavljevic, V. Oja, E.M. Suuberg, Thermal effects in cellulose pyrolysis: Relationship to char formation processes, Ind. Eng. Chem. Res. 35 (3) (1996) 653–662, https://doi.org/10.1021/ie950438l.

[30] W.S.L. Mok, M.J. Antal, Effects of pressure on biomass pyrolysis 2. Heats of reaction of cellulose pyrolysis, Thermochim. Acta 68 (2–3) (1983) 165–186, https://doi.org/10.1016/0040-6031(83)80222-6.

[31] W.S.L. Mok, M.J. Antal, Effects of pressure on biomass pyrolysis i. cellulose pyrolysis products, Thermochim. Acta 68 (2–3) (1983) 155–164, https://doi.org/10.1016/0040-6031(83)80221-4.

[32] R. Narayan, M.J. Antal, Thermal lag, fusion, and the compensation effect during biomass pyrolysis, Ind. Eng. Chem. Res. 35 (5) (1996) 1711–1721, https://doi.org/10.1021/ie950368i.

[33] G. Varhegyi, M.J. Antal, T. Szekely, F. Till, E. Jakab, P. Szabo, Simultaneous thermogravimetric mass-spectrometric studies of the thermal-decomposition of bio-polymers.2. sugar-cane bagasse in the presence and absence of catalysts, Energ. Fuel 2 (3) (1988) 273–277, https://doi.org/10.1021/ef00009a008.

[34] G. Varhegyi, P. Szabo, M.J. Antal, Kinetics of the Thermal-decomposition of cellulose under the experimental conditions of thermal-analysis - theoretical extrapolations to high heating rates, Biomass Bioenerg. 7 (1–6) (1994) 69–74, https://doi.org/10.1016/0961-9534(95)92631-H.

[35] I. Pastorova, R.E. Botto, P.W. Arisz, J.J. Boon, Cellulose char structure - a combined analytical Py-GC-MC, FTIR, and NMR-study, Carbohydr. Res. 262 (1) (1994) 27–47, https://doi.org/10.1016/0008-6215(94)84003-2.

[36] P.R. Patwardhan, D.L. Dalluge, B.H. Shanks, R.C. Brown, Distinguishing primary and secondary reactions of cellulose pyrolysis, Bioresour. Technol. 102 (8) (2011) 5265–5269, https://doi.org/10.1016/j.biortech.2011.02.018.

[37] S.R. Wang, X.J. Guo, T. Liang, Y. Zhou, Z.Y. Luo, Mechanism research on cellulose pyrolysis by Py-GC/MS and subsequent density functional theory studies, Bioresour. Technol. 104 (2012) 722–728, https://doi.org/10.1016/j.biortech.2011.10.078.

[38] M.M. Tang, R. Bacon, Carbonization of cellulose fibers.1. Low temperature pyrolysis, Carbon 2 (3) (1964) 211, https://doi.org/10.1016/0008-6223(64)90035-1.

[39] P. Jusner, M. Bacher, J. Simon, F. Bausch, H. Khaliliyan, S. Schiehser, I. Sumerskii, E. Schwaiger, A. Potthast, T. Rosenau, Analyzing the effects of thermal stress on insulator papers by solid-state ^{13}C NMR spectroscopy, Cellulose 29 (2) (2022) 1081–1095, https://doi.org/10.1007/s10570-021-04338-z.

[40] H. Knicker, M. Velasco-Molina, M. Knicker, 2D solid-state HETCOR ^{1}H–^{13}C NMR experiments with variable cross polarization times as a tool for a better understanding of the chemistry of cellulose-based pyrochars-a tutorial, Appl. Sci.-Basel 11 (18) (2021), https://doi.org/10.3390/app11188569.

[41] H. Plaisantin, R. Pailler, A. Guette, G. Daude, M. Petraud, B. Barbe, M. Birot, J. P. Pillot, P. Olry, Conversion of cellulosic fibres into carbon fibres: a study of the mechanical properties and correlation with chemical structure, Compos. Sci. Technol. 61 (14) (2001) 2063–2068, https://doi.org/10.1016/S0266-3538(01)00107-5.

[42] J. Zawadzki, M. Wisniewski, ^{13}C NMR study of cellulose thermal treatment, J. Anal. Appl. Pyrol 62 (1) (2002) 111–121, https://doi.org/10.1016/S0165-2370(00)00217-5.

[43] G.J. Kwon, D.Y. Kim, K.Y. Kang, Effects of low-temperature pretreatment on carbonization of cellulose for the production of biocarbons, J. Korean Phys. Soc. 60 (10) (2012) 1814–1817, https://doi.org/10.3938/jkps.60.1814.

[44] J. Scheirs, G. Camino, W. Tumiatti, Overview of water evolution during the thermal degradation of cellulose, Eur. Polym. J. 37 (5) (2001) 933–942, https://doi.org/10.1016/S0014-3057(00)00211-1.

[45] A.G. Dumanli, A.H. Windle, Carbon fibres from cellulosic precursors: a review, J. Mater. Sci. 47 (10) (2012) 4236–4250, https://doi.org/10.1007/s10853-011-6081-8.

[46] Y. Long, Y. Yu, Y.W. Chua, H.W. Wu, Acid-catalysed cellulose pyrolysis at low temperatures, Fuel 193 (2017) 460–466, https://doi.org/10.1016/j.fuel.2016.12.067.

[47] D.Y. Kim, Y. Nishiyama, M. Wada, S. Kuga, High-yield carbonization of cellulose by sulfuric acid impregnation, Cellulose 8 (1) (2001) 29–33, https://doi.org/10.1023/A:1016621103245.

[48] G. Dobele, G. Rossinskaja, G. Telysheva, D. Meier, O. Faix, Cellulose dehydration and depolymerization reactions during pyrolysis in the presence of phosphoric acid, J. Anal. Appl. Pyrol. 49 (1–2) (1999) 307–317, https://doi.org/10.1016/S0165-2370(98)00126-0.

[49] M.J. Antal, Biomass pyrolysis: a review of the literature part 1—carbohydrate pyrolysis, in: K.W. Böer, J.A. Duffie (Eds.), Advances in Solar Energy, Springer, Boston, MA, 1983.

[50] I. Pastorova, P.W. Arisz, J.J. Boon, Preservation of D-glucose-oligosaccharides in cellulose chars, Carbohydr. Res. 248 (1993) 151–165, https://doi.org/10.1016/0008-6215(93)84123-N.

[51] N.S. Hon, Formation of free-radicals in photoirradiated cellulose.1. Effect of wavelength, J. Polym. Sci. Pol. Chem. 13 (6) (1975) 1347–1361, https://doi.org/10.1002/pol.1975.170130607.

[52] N.S. Hon, Formation of free-radicals in photoirradiated cellulose.2. Effect of moisture, J. Polym. Sci. Pol. Chem. 13 (4) (1975) 955–959, https://doi.org/10.1002/pol.1975.170130414.

[53] R.S. Parikh, Reaction mechanism involved in cross-linking formaldehyde and RCH2OH with cellulose, Text. Res. J. 37 (6) (1967) 538, https://doi.org/10.1177/004051756703700618.

[54] X.L. Bai, P. Johnston, S. Sadula, R.C. Brown, Role of levoglucosan physiochemistry in cellulose pyrolysis, J. Anal. Appl. Pyrol. 99 (2013) 58–65, https://doi.org/10.1016/j.jaap.2012.10.028.

[55] E.W. Leng, M. Costa, Y. Peng, Y. Zhang, X. Gong, A.Q. Zheng, Y.Q. Huang, M. H. Xu, Role of different chain end types in pyrolysis of glucose-based anhydro-sugars and oligosaccharides, Fuel 234 (2018) 738–745, https://doi.org/10.1016/j.fuel.2018.07.075.

[56] Q. Lu, B. Hu, Z.X. Zhang, Y.T. Wu, M.S. Cui, D.J. Liu, C.Q. Dong, Y.P. Yang, Mechanism of cellulose fast pyrolysis: The role of characteristic chain ends and dehydrated units, Combust. Flame 198 (2018) 267–277, https://doi.org/10.1016/j.combustflame.2018.09.025.

[57] S. Matsuoka, H. Kawamoto, S. Saka, Thermal glycosylation and degradation reactions occurring at the reducing ends of cellulose during low-temperature pyrolysis, Carbohydr. Res. 346 (2) (2011) 272–279, https://doi.org/10.1016/j.carres.2010.10.018.

[58] S. Matsuoka, H. Kawamoto, S. Saka, What is active cellulose in pyrolysis? An approach based on reactivity of cellulose reducing end, J. Anal. Appl. Pyrol. 106 (2014) 138–146, https://doi.org/10.1016/j.jaap.2014.01.011.

[59] T. Hosoya, S. Sakaki, Levoglucosan formation from crystalline cellulose: importance of a hydrogen bonding network in the reaction, Chemsuschem 6 (12) (2013) 2356–2368, https://doi.org/10.1002/cssc.201300338.

[60] M.L. Wolfrom, A. Thompson, R.B. Ward, The composition of pyrodextrins.2. Thermal polymerization of levoglucosan, J. Am. Chem. Soc. 81 (17) (1959) 4623–4625, https://doi.org/10.1021/ja01526a043.

[61] M.L. Wolfrom, R.B. Ward, D. Horton, R.H. Moore, A. Thompson, Composition of pyrodextrins.3. Thermal polymerization of levoglucosan, J. Org. Chem. 26 (11) (1961) 4617, https://doi.org/10.1021/jo01069a099.

[62] Y. Houminer, S. Patai, Thermal polymerization of levoglucosan, J. Polym. Sci. A1 7 (10) (1969) 3005, https://doi.org/10.1002/pol.1969.150071020.

[63] H. Kawamoto, M. Murayama, S. Saka, Pyrolysis behavior of levoglucosan as an intermediate in cellulose pyrolysis: polymerization into polysaccharide as a key reaction to carbonized product formation, J. Wood Sci. 49 (5) (2003) 469–473, https://doi.org/10.1007/s10086-002-0487-5.

[64] F. Shafizadeh, R.H. Furneaux, T.T. Stevenson, T.G. Cochran, Acid-catalyzed pyrolytic synthesis and decomposition of 1,4-3,6-dianhydro-alpha-D-glucopyranose, Carbohydr. Res 61 (3) (1978) 519–528, https://doi.org/10.1016/S0008-6215(00)84510-3.

[65] N.D. Le, M. Trogen, Y.B. Ma, R.J. Varley, M. Hummel, N. Byrne, Cellulose-lignin composite fibers as precursors for carbon fibers: Part 2-The impact of precursor properties on carbon fibers, Carbohydr. Polym. 250 (2020), https://doi.org/10.1016/j.carbpol.2020.116918.

[66] J. Mikkila, M. Trogen, K.A.Y. Koivu, J. Kontro, J. Kuuskeri, R. Maltari, Z. Dekere, M. Kemell, M.R. Makela, P.A. Nousiainen, M. Hummel, J. Sipila, K. Hilden, Fungal treatment modifies kraft lignin for lignin- and cellulose-based carbon fiber precursors, ACS Omega 5 (11) (2020) 6130–6140, https://doi.org/10.1021/acsomega.0c00142.

[67] H. Zahra, D. Sawada, C. Guizani, Y.B. Ma, S. Kumagai, T. Yoshioka, H. Sixta, M. Hummel, Close packing of cellulose and chitosan in regenerated cellulose fibers improves carbon yield and structural properties of respective carbon fibers, Biomacromolecules 21 (10) (2020) 4326–4335, https://doi.org/10.1021/acs.biomac.0c01117.

[68] M. Trogen, N.D. Le, D. Sawada, C. Guizani, T.V. Lourencon, L. Pitkanen, H. Sixta, R. Shah, H. O'Neill, M. Balakshin, N. Byrne, M. Hummel, Cellulose-lignin composite fibres as precursors for carbon fibres. Part 1-Manufacturing and

properties of precursor fibres, Carbohydr. Polym. 252 (2021), https://doi.org/10.1016/j.carbpol.2020.117133.

[69] L. Fliri, K. Heise, T. Koso, A.R. Todorov, D.R. del Cerro, S. Hietala, J. Fiskari, I. Kilpeläinen, M. Hummel, A.W.T. King, Solution-state nuclear magnetic resonance spectroscopy of crystalline cellulosic materials using a direct dissolution ionic liquid electrolyte, Nat. Protoc. 18 (2023) 2084–2123, https://doi.org/10.1038/s41596-023-00832-9.

[70] T. Koso, D.R. del Cerro, S. Heikkinen, T. Nypelo, J. Buffiere, J.E. Perea-Buceta, A. Potthast, T. Rosenau, H. Heikkinen, H. Maaheimo, A. Isogai, I. Kilpelainen, A. W.T. King, 2D Assignment and quantitative analysis of cellulose and oxidized celluloses using solution-state NMR spectroscopy, Cellulose 27 (14) (2020) 7929–7953, https://doi.org/10.1007/s10570-020-03317-0.

[71] A.W.T. King, V. Makela, S.A. Kedzior, T. Laaksonen, G.J. Partl, S. Heikkinen, H. Koskela, H.A. Heikkinen, A.J. Holding, E.D. Cranston, I. Kilpelainen, Liquid-state NMR analysis of nanocelluloses, Biomacromolecules 19 (7) (2018) 2708–2720, https://doi.org/10.1021/acs.biomac.8b00295.

[72] C. Guizani, S. Larkiala, K. Moriam, D. Sawada, S. Elsayed, S. Rantasalo, M. Hummel, H. Sixta, Air gap spinning of a cellulose solution in [DBNH][OAc] ionic liquid with a novel vertically arranged spinning bath to simulate a closed loop operation in the Ioncell (R) process, J. Appl. Polym. Sci. 138 (5) (2021), https://doi.org/10.1002/app.49787.

[73] A. Michud, M. Hummel, H. Sixta, Influence of process parameters on the structure formation of man-made cellulosic fibers from ionic liquid solution, J. Appl. Polym. Sci. 133 (30) (2016), https://doi.org/10.1002/app.43718.

[74] H. Sixta, A. Michud, L. Hauru, S. Asaadi, Y.B. Ma, A.W.T. King, I. Kilpelainen, M. Hummel, Ioncell-F: a high-strength regenerated cellulose fibre, Nord. Pulp. Pap. Res. J. 30 (1) (2015) 43–57, https://doi.org/10.3183/npprj-2015-30-01-p043-057.

[75] S. Asaadi, M. Hummel, P. Ahvenainen, M. Gubitosi, U. Olsson, H. Sixta, Structural analysis of Ioncell-F fibres from birch wood, Carbohydr. Polym. 181 (2018) 893–901, https://doi.org/10.1016/j.carbpol.2017.11.062.

[76] S.C. Yuan, M.V. Tyufekchiev, M.T. Timko, K. Schmidt-Rohr, Direct quantification of the degree of polymerization of hydrolyzed cellulose by solid-state NMR spectroscopy, Cellulose 29 (4) (2022) 2131–2144, https://doi.org/10.1007/s10570-022-04433-9.

[77] M. Maciejewski, A. Baiker, Quantitative calibration of mass spectrometric signals measured in coupled TA-MS system, Thermochim. Acta 295 (1–2) (1997) 95–105, https://doi.org/10.1016/S0040-6031(97)00100-7.

[78] F. D'Acierno, W.Y. Hamad, C.A. Michal, M.J. MacLachlan, Thermal degradation of cellulose filaments and nanocrystals, Biomacromolecules 21 (8) (2020) 3374–3386, https://doi.org/10.1021/acs.biomac.0c00805.

[79] N. Atykyan, V. Revin, V. Shutova, Raman and FT-IR Spectroscopy investigation the cellulose structural differences from bacteria Gluconacetobacter sucrofermentans during the different regimes of cultivation on a molasses media, Amb. Express 10 (1) (2020), https://doi.org/10.1186/s13568-020-01020-8.

[80] S. Asaadi, T. Kakko, A.W.T. King, I. Kilpelainen, M. Hummel, H. Sixta, High-performance acetylated ioncell-f fibers with low degree of substitution, ACS Sustain. Chem. Eng. 6 (7) (2018) 9418–9426, https://doi.org/10.1021/acssuschemeng.8b01768.

[81] L. Pitkanen, H. Sixta, Size-exclusion chromatography of cellulose: observations on the low-molar-mass fraction, Cellulose 27 (16) (2020) 9217–9225, https://doi.org/10.1007/s10570-020-03419-9.

[82] T. Rosenau, A. Potthast, W. Milacher, A. Hofinger, P. Kosma, Isolation and identification of residual chromophores in cellulosic materials, Polymer 45 (19) (2004) 6437–6443, https://doi.org/10.1016/j.polymer.2004.07.031.

[83] P. Jusner, F. Bausch, S. Schiehser, E. Schwaiger, A. Potthast, T. Rosenau, Protocol for characterizing the molar mass distribution and oxidized functionality profiles of aged transformer papers by gel permeation chromatography (GPC), Cellulose 29 (4) (2022) 2241–2256, https://doi.org/10.1007/s10570-022-04464-2.

[84] S.L. Madorsky, V.E. Hart, S. Straus, Thermal degradation of cellulosic materials, J. Res. Nat. Bur. Stand. 60 (4) (1958) 343–349.

[85] F.J. Kilzer, A. Broido, Speculations on nature of cellulose pyrolysis, Pyrodynamics 2 (1965) 151–163.

[86] T. Hosoya, M. Bacher, A. Potthast, T. Elder, T. Rosenau, Insights into degradation pathways of oxidized anhydroglucose units in cellulose by beta-alkoxy-elimination: a combined theoretical and experimental approach, Cellulose 25 (7) (2018) 3797–3814, https://doi.org/10.1007/s10570-018-1835-y.

[87] J. Simon, L. Fliri, J. Sapkota, M. Ristolainen, S.A. Miller, M. Hummel, T. Rosenau, A. Potthast, Reductive amination of dialdehyde cellulose: access to renewable thermoplastics, Biomacromolecules 24 (1) (2023) 166–177, https://doi.org/10.1021/acs.biomac.2c01022.

[88] T. Koso, M. Beaumont, B.L. Tardy, D.R. del Cerro, S. Eyley, W. Thielemans, O. J. Rojas, I. Kilpelainen, A.W.T. King, Highly regioselective surface acetylation of cellulose and shaped cellulose constructs in the gas-phase, Green Chem. 24 (14) (2022) 5604–5613, https://doi.org/10.1039/D2GC01141G.

[89] M. Beaumont, C.G. Otoni, B.D. Mattos, T.V. Koso, R. Abidnejad, B. Zhao, A. Kondor, A.W.T. King, O.J. Rojas, Regioselective and water-assisted surface esterification of never-dried cellulose: nanofibers with adjustable surface energy, Green. Chem. 23 (18) (2021) 6966–6974, https://doi.org/10.1039/D1GC02292J.

[90] D. Gardiner, The pyrolysis of some hexoses and derived di-, tri-, and poly-saccharides, J. Chem. Soc. C. (1966) 1473–1476, https://doi.org/10.1039/J39660001473.

[91] H.P. Yang, R. Yan, H.P. Chen, D.H. Lee, C.G. Zheng, Characteristics of hemicellulose, cellulose and lignin pyrolysis, Fuel 86 (12–13) (2007) 1781–1788, https://doi.org/10.1016/j.fuel.2006.12.013.

[92] F.X. Collard, J. Blin, A review on pyrolysis of biomass constituents: Mechanisms and composition of the products obtained from the conversion of cellulose, hemicelluloses and lignin, Renew. Sust. Energ. Rev. 38 (2014) 594–608, https://doi.org/10.1016/j.rser.2014.06.013.

[93] X. Zhou, W. Li, R. Mabon, L.J. Broadbelt, A Critical Review on Hemicellulose Pyrolysis Energy Technol. 5(1) (2017) 52–79, https://doi.org/10.1002/ente.201600327.

[94] H. Hatakeyama, T. Hatakeyama, Interaction between water and hydrophilic polymers, Thermochim. Acta 308 (1–2) (1998) 3–22, https://doi.org/10.1016/S0040-6031(97)00325-0.

[95] L. Geminiani, F.P. Campione, C. Corti, M. Luraschi, S. Motella, S. Recchia, L. Rampazzi, Differentiating between natural and modified cellulosic fibres using ATR-FTIR, Spectrosc., Herit. 5 (4) (2022) 4114–4139, https://doi.org/10.3390/heritage5040213.

[96] S.Y. Oh, D.I. Yoo, Y. Shin, H.C. Kim, H.Y. Kim, Y.S. Chung, W.H. Park, J.H. Youk, Crystalline structure analysis of cellulose treated with sodium hydroxide and carbon dioxide by means of X-ray diffraction and FTIR spectroscopy, Carbohydr. Res. 340 (15) (2005) 2376–2391, https://doi.org/10.1016/j.carres.2005.08.007.

[97] Y. Marechal, H. Chanzy, The hydrogen bond network in I-beta cellulose as observed by infrared spectrometry, J. Mol. Struct. 523 (2000) 183–196, https://doi.org/10.1016/S0022-2860(99)00389-0.

[98] A.M. Striegel, Modern Size-exclusion Liquid Chromatography: Practice of Gel Permeation and Gel Filtration Chromatography, 2nd ed..,, Wiley,, Hoboken, N.J, 2009.

[99] W. Burchard, Solution properties of branched macromolecules, Adv. Polym. Sci. 143 (1999) 113–194, https://doi.org/10.1007/3-540-49780-3_3.

[100] H. Kawamoto, Review of reactions and molecular mechanisms in cellulose pyrolysis, Curr. Org. Chem. 20 (23) (2016) 2444–2457, https://doi.org/10.2174/2213337203666160525102910.